vehicles

MDPI

Article

Safety-Oriented Comparative Assessment of Autonomous Path-Tracking Controllers Using a Real-World-Validated Virtual Vehicle Model

Efe Savran

Mechanical Engineering Department, Bursa Uludag University, 16059 Bursa, Turkey; efesavran@uludag.edu.tr

Abstract

Comparisons of path-tracking controllers based mainly on tracking error may overlook differences in steering activity, vehicle response, and lane containment. This study compares Pure Pursuit, Stanley, and Model Predictive Control using a common virtual vehicle model and multiple safety-related performance indicators. The virtual vehicle model was evaluated against two separate CAN recordings from the same vehicle without recalibration between evaluations. Vehicle-speed and front-wheel-speed predictions showed R^2 values above 0.97 in both recordings; yaw-rate R^2 values were 0.957 and 0.930, whereas lateral-acceleration agreement was lower, particularly in the second recording. A Common Path Manager provided consistent reference-path information and steering constraints for all three controllers. They were evaluated at 5 and 10 km/h on idealized hairpin and spiral paths using tracking errors, steering-command-rate RMS, kinematic-response measures, and center-of-gravity-based and sampled vehicle-body lane-containment measures. MPC achieved the lowest cross-track-error RMSE in both scenarios, whereas Pure Pursuit produced the lowest steering-command-rate, lateral-acceleration, and yaw-rate RMS values. Stanley achieved the lowest heading-error RMSE in the spiral scenario. In the hairpin tests, the vehicle center of gravity remained within the lane for all controllers, although the body was partially outside the modeled lane corridor in 37.048–53.352% of evaluated samples. These findings show that lower tracking error does not necessarily coincide with lower steering-command activity or improved CG-based lane keeping. The evaluated quantities are safety-related performance indicators for the investigated simulation conditions and do not constitute a comprehensive assessment of vehicle safety.

Keywords: autonomous driving; path tracking; surrogate safety measurement; pure pursuit; Stanley; model predictive control

Check for updates

Academic Editor: Ralf Stetter

Received: 4 September 2026
Revised: 27 September 2026
Accepted: 1 October 2026
Published: 5 October 2026

Copyright: © 2026 by the author. Licensee MDPI, Basel, Switzerland. This article is an open access article distributed under the terms and conditions of the Creative Commons Attribution (CC BY) license.

1. Introduction

The ability of autonomous vehicles to proceed safely on the determined route depends on a properly functioning lateral control mechanism [1]. Especially in sharp bends and low-speed maneuvers, path-tracking controllers become the cornerstone of driving [2]. Poor lateral control leads to deviations from the route, unnecessary steering interventions, and the risk of the vehicle leaving the lane. Therefore, when measuring the success of a controller, it is necessary to look not only at how accurately it follows the route, but also at the physical reactions of the vehicle while doing this tracking [3].

Although many methods have been proposed for lateral control in autonomous vehicles, Pure Pursuit, Stanley, and Model Predictive Control are three approaches that stand

out in the literature [4]. Pure Pursuit determines the steering angle entirely through geometric calculations by focusing on a defined target point in front of the vehicle [4]. Stanley generates the steering command by simultaneously taking into account the heading error and how much it deviates from the lane [5]. Model Predictive Control differs from these two methods, which work with geometric logic. It predicts the movement of the vehicle in future steps within a certain time interval, and optimizes and applies the most suitable steering command sequence in line with the defined constraints and targets [4].

Previous comparative studies have primarily focused on lateral tracking and steering errors when ranking road tracking controllers [6]. Although some studies have also considered additional quantifiers such as yaw response, steering movement, lateral acceleration, and road limit constraints, controller performance is still often summarized using a limited number of tracking error metrics [1].

It is hard to state that a controller that reduces lateral deviation to near zero will also provide the smoothest steering movements or the calmest vehicle dynamics. In fact, in the literature, path-tracking accuracy and how sharply or quickly the steering intervenes are treated as separate and potentially conflicting objectives [7]. On the other hand, a low average tracking error alone does not guarantee that the vehicle remains safely within the lane boundaries throughout the maneuver. Therefore, constraints such as outside-lane ratio and vehicle stability are treated as parameters independent of deviation error in most control approaches [8]. This situation becomes particularly evident on challenging routes where the curve radius is small. This is because increasing road curvature increases the load on the steering and makes the balance that the controller establishes between tracking accuracy and vehicle responses much more critical [9].

To mitigate the impact of platform-dependent differences, controller comparisons should ideally be performed using the same vehicle model, reference road guidance, and operating conditions [1]. Furthermore, validating the common vehicle platform using real-world vehicle measurements can provide a more representative basis than relying solely on an unvalidated simulation model.

Despite extensive research on Pure Pursuit, Stanley, and Model Predictive Control, comparative studies are needed to evaluate these controllers on a common real-world validated vehicle platform, using both traditional tracking metrics and complementary metrics such as steering command activity, kinematic vehicle response, and lane keeping. This is particularly important for geometrically challenging low-speed maneuvers, where controllers can achieve comparable path-tracking performance with significantly different steering and vehicle response characteristics. Artuñedo et al. [1] noted a lack of comprehensive comparisons of different lateral controllers under the same tuning methodology using simulations and real vehicle tests, and therefore performed a systematic comparison with a broader set of metrics including accuracy, robustness, and comfort. Rumetshofer et al. [10] showed that even reference-path representation affects the final tracking performance when evaluating different controllers within the same path-tracking framework. They noted that Pure Pursuit produces lower steering effort but higher lateral error, while Stanley achieves better tracking at the expense of higher steering effort. Jung [11] explained that Pure Pursuit and Stanley controllers exhibit different tracking and steering-response characteristics under curved-path conditions; for example, increasing the look-ahead distance can produce a smoother response but corner cutting, while decreasing it can produce higher tracking accuracy but steering oscillation. Lee and Yim [3] compared different path-tracking controllers such as Pure Pursuit, Stanley, PID, Linear–Quadratic Regulator, Sliding Mode Control, and Model Predictive Control in the same vehicle simulation environment under low-friction road conditions. In the reference, controller performance was evaluated not only through lateral tracking error but also using path-tracking performance, steering effort, and lateral

stability criteria. The authors showed that it is not sufficient to consider a controller superior only based on tracking accuracy, and that steering effort and lateral stability behaviors should also be included in the evaluation. Hossain et al. [12] comparatively evaluated various path-tracking approaches, including Pure Pursuit, Stanley, Linear–Quadratic Regulator, and Model Predictive Control, under common trajectory tracking conditions. In addition to lateral tracking error, the study also evaluated steering angle and yaw angle responses at different path geometries. The results showed that controller behavior, especially during sharp cornering maneuvers, cannot be characterized solely by lateral tracking accuracy.

The objective of this study is to compare the implemented Pure Pursuit, Stanley, and Model Predictive Control (MPC) controllers under common low-speed test conditions and to examine how conclusions based on tracking accuracy differ from those based on steering-command activity, kinematic response, and lane containment. The comparison uses a virtual vehicle model evaluated against two separate CAN recordings from the same vehicle. The controllers are tested at 5 and 10 km/h on hairpin and spiral reference paths, which serve as idealized geometric stress tests.

The study contributes a Common Path Manager that provides consistent path localization, path-progress information, vehicle geometry, and steering-angle limits to the three controller implementations. It also evaluates controller behavior using complementary measures of tracking error, steering-command activity, lateral acceleration, yaw rate, and lane containment. Lane containment is assessed using both the vehicle center of gravity and sampled vehicle-body footprints, allowing cases in which the center of gravity remains inside the lane while part of the body extends beyond it to be identified. The resulting comparison describes the trade-offs of the specified controller configurations under the investigated simulation conditions; it does not establish a universally superior controller or the best attainable performance of each control strategy.

2. Materials and Methods

The methodology followed five main stages: real data acquisition, virtual vehicle model development and validation, integration of path-tracking controllers, identification of common test scenarios, and comprehensive performance evaluation. The model was evaluated using two separate CAN recordings of 331 and 780 s obtained from the same vehicle under comparable driving conditions. The recordings contained vehicle speed, front-wheel speeds, steering-wheel angle, lateral acceleration, and yaw rate. Then, based on the real vehicle's physical and geometric dimensions, a virtual vehicle model was created in MATLAB/Simulink R2022b, including longitudinal force–velocity calculations, steering system, Ackermann angle, and lateral responses. In the validation phase, the speed profile and steering angle obtained from the real test were given as input to the model. The results obtained from the simulation were compared with the CAN data using RMSE, MAE, R^2, and Pearson correlation coefficients. Pure Pursuit, Stanley, and Model Predictive Control methods were tested on the validated model. A Common Path Manager was designed to allow the controllers to compete under equal conditions. This structure fed all algorithms with the same reference route, positioning, cross-track error, directional information, and steering constraints. All algorithms were tested under the same vehicle conditions on two challenging routes: a hairpin path with sharp 90-degree turns and a spiral path that progressively moves inward. The tests were repeated at constant speeds of 5 and 10 km/h. To avoid reducing performance to a single criterion, parameters such as cross-track error and heading RMSE values, steering-command-rate RMS, lateral acceleration, yaw rate, outside-lane ratio, and lane margin were evaluated together. Thus, not only tracking accuracy but also lane-keeping success, steering intensity,

and the vehicle's dynamic responses were measured holistically. Figure 1 illustrates the stages of the methodology.

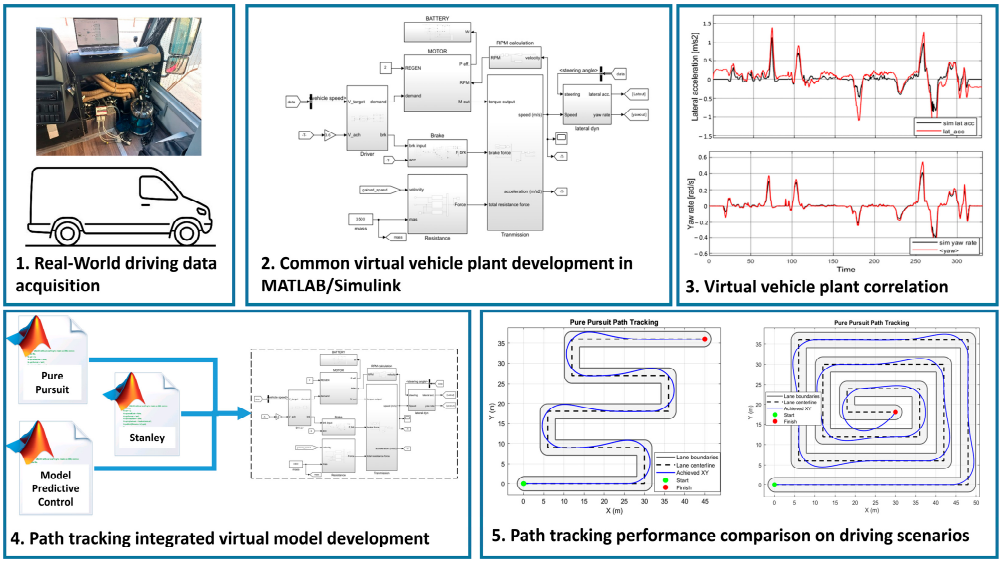


Figure 1. Workflow of the study.

2.1. Data Acquisition

The driving data were collected from an electric VAN. The VECTOR tool was connected to the vehicle control unit through the OBD-II port, and CAN signals transmitted via the SAE J1939 protocol were recorded using the CANAlyzer 15 software. The CAN signals were recorded at a sampling interval of 0.1 s. The recorded signals included vehicle speed (km/h), front-left and front-right wheel speeds (km/h), lateral acceleration (m/s^2), yaw rate (rad/s), and steering-wheel angle (rad).

The first road test followed the route shown in Figure 2 and lasted 331 s. It was conducted in sunny, calm, and dry weather on a route free of traffic. A single driver performed the test to minimize driver-dependent variability. A second, separate 780 s recording was obtained from the same vehicle under the same driving conditions and was used for an additional validation of the unchanged virtual vehicle model. The recorded signals were exported as CSV files and subsequently converted to XLSX format for data processing and model validation. No filtering was applied to the measured signals before validation.

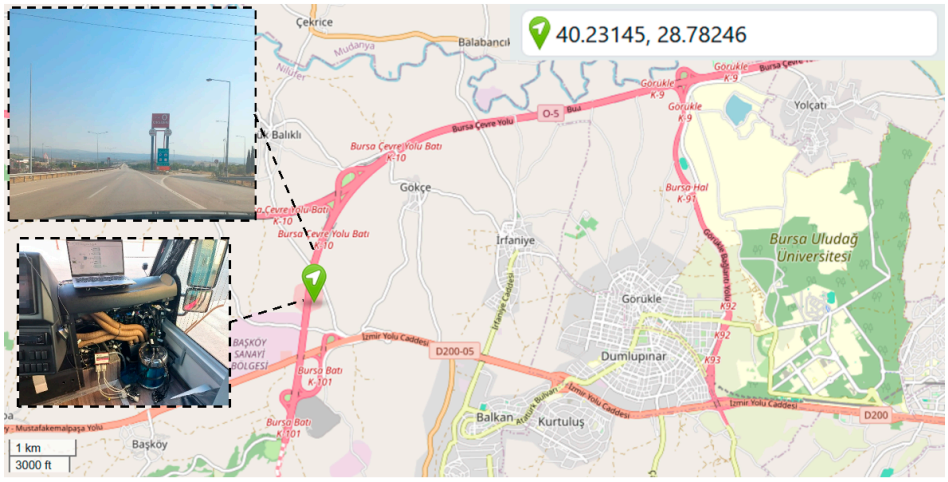


Figure 2. Location and route used for real-world CAN data acquisition (Map: ©OpenStreetMap contributors [13]).

The e-VAN platform used in this model has a gross mass range of 3000–5500 kg and is equipped with an 82 kWh battery and an electric motor with approximately 300 Nm of peak torque. The model utilizes tires with an effective rolling radius of 0.36 m, a frontal area of 5.5 m^2, an aerodynamic drag coefficient (Cd) of 0.34, and a rolling resistance coefficient (Crr) of 0.007. The vehicle geometry is based on a wheelbase (WB) of 3.745 m, a front track width (TW) of 1.810 m, a steering-pivot width (wp) of 1.666 m, and a front tire tread width of 0.215 m. The distances from the center of gravity (CG) to the front and rear axles are 1.870 m and 1.880 m, respectively, and the CG height is 0.948 m. To preserve commercial confidentiality, the vehicle manufacturer and commercial model are not disclosed.

2.2. Common Virtual Vehicle Plant Development

In this study, the vehicle virtual platform used for the comparison of tracking controllers utilized the basic equations of motion. According to Newton's second law, motion begins when the resistance forces on a system are overcome, and the resistance forces given in the study by Savran et al. [14] were used. The vehicle output velocity (Vx) is given in its simplest form in Equation (1), where V_x is the vehicle longitudinal velocity, F_{tr} is the force from the traction system, F_{br} is the braking force, and F_r is the total resistance force.

$$V_x(t) = V_x(t_0) + \int_0^t \frac{F_{tr} - F_{br} - F_r}{m} dt \tag{1}$$

In the rack displacement (x_{track}) calculation in Equation (2), the rack displacement gain value (k_{rack}) is taken as 7 mm/rad. The δ_{str} is the steering angle input.

$$x_{track} = k_{rack}\delta_{str} \tag{2}$$

The mean front-wheel angle (δ_m) is found according to Equation (3), and the distance between the pivot and the wheel center of rotation (lk) is 146.75 mm.

$$\delta_m = \sin^{-1}\left(\frac{x_{track}}{l_k}\right) \tag{3}$$

The mean turning radius (R) is calculated according to 4. The δ_m is the mean wheel angle in radians.

$$R = \frac{WB}{\tan(\delta_m)} \tag{4}$$

The left and right tire turning radii (R_L and R_R) are calculated according to Equation (5). The distance between the turning points of the steering wheels (w_p) was used.

$$\begin{aligned} R_L &= R - \tfrac{w_p}{2} \\ R_R &= R + \tfrac{w_p}{2} \end{aligned} \tag{5}$$

The Ackermann left and right wheel angles (δ_L and δ_R) are calculated according to Equation (6).

$$\begin{aligned} \delta_L &= \tan^{-1}\left(\tfrac{WB}{R_L}\right) \\ \delta_R &= \tan^{-1}\left(\tfrac{WB}{R_R}\right) \end{aligned} \tag{6}$$

The left and right front-wheel speeds (V_{FL} and V_{FR}) are found in Equation (7).

$$V_{FL} = \sqrt{\left(V_x - \frac{rTW}{2}\right)^2 + (rWB)^2}$$
$$V_{FR} = \sqrt{\left(V_x + \frac{rTW}{2}\right)^2 + (rWB)^2} \quad (7)$$

In calculating lateral acceleration (a_y), one of the kinematic lateral-response outputs, both V_x and R are required. The basic calculation approach for lateral acceleration is given in Equation (8).

$$a_y = \frac{{V_x}^2}{R} \quad (8)$$

The yaw-rate (r) calculation is given in Equation (9).

$$r = \frac{V_x}{WB} \tan \delta_m \quad (9)$$

The theoretical approach presented in Equations (1)–(9) has been implemented in the MATLAB/Simulink R2022b platform, as shown in Figure 3, taking into account previous studies [15]. In the virtual platform created considering the physical conditions of the e-VAN from which driving data is obtained, linear and lateral acceleration (m/s^2), yaw rate (rad/s), and right and left wheel speeds (km/h) are obtained in response to the vehicle-speed target (km/h) and steering angle (rad) inputs. On the virtual platform, the driver subsystem decides on motor torque or braking demand in response to the entered speed target. Simultaneously, the dominant force is determined by combining it with the vehicle's resistance force. Acceleration and speed outputs are obtained from the net force, and the speed information is transmitted to the necessary subsystems. Lateral acceleration and yaw rate values are calculated using speed and steering angle inputs. The energy consumption value can also be obtained as an output from the motor subsystem.

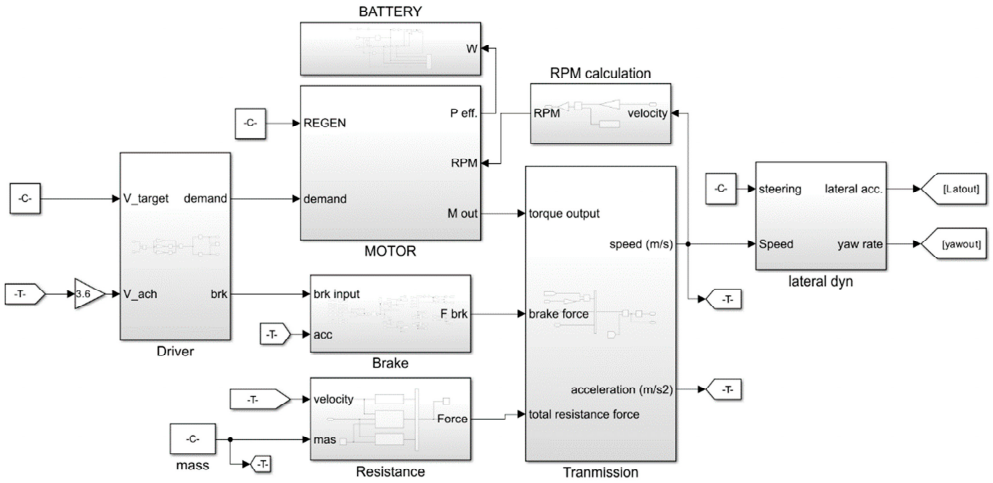


Figure 3. Real-world validated virtual vehicle model.

For each recording, the measured CAN vehicle-speed profile was supplied to the virtual driver subsystem as the target-speed input, while the measured steering-wheel-angle signal was supplied to the steering subsystem through the same rack and steering geometry. The resulting simulated vehicle speed, front-left and front-right wheel speeds, yaw rate, and lateral acceleration were compared with their corresponding CAN measurements using RMSE, MAE, R^2, and Pearson's correlation coefficient. The 331 s recording was

evaluated first, followed by the separate 780 s recording. The model equations, parameters, and subsystem settings were not changed or recalibrated between the two evaluations.

Figure 4 shows a visual representation of the vehicle's average speed, left and right wheel speeds, lateral acceleration, and yaw-rate outputs in response to input speed and steering angle commands given on the virtual vehicle platform. In the visuals, red lines represent data obtained from real driving, while black lines represent the virtual vehicle platform outputs. As can be seen from the visuals, the behavior of the prepared virtual platform is similar to the driving behavior of the real vehicle.

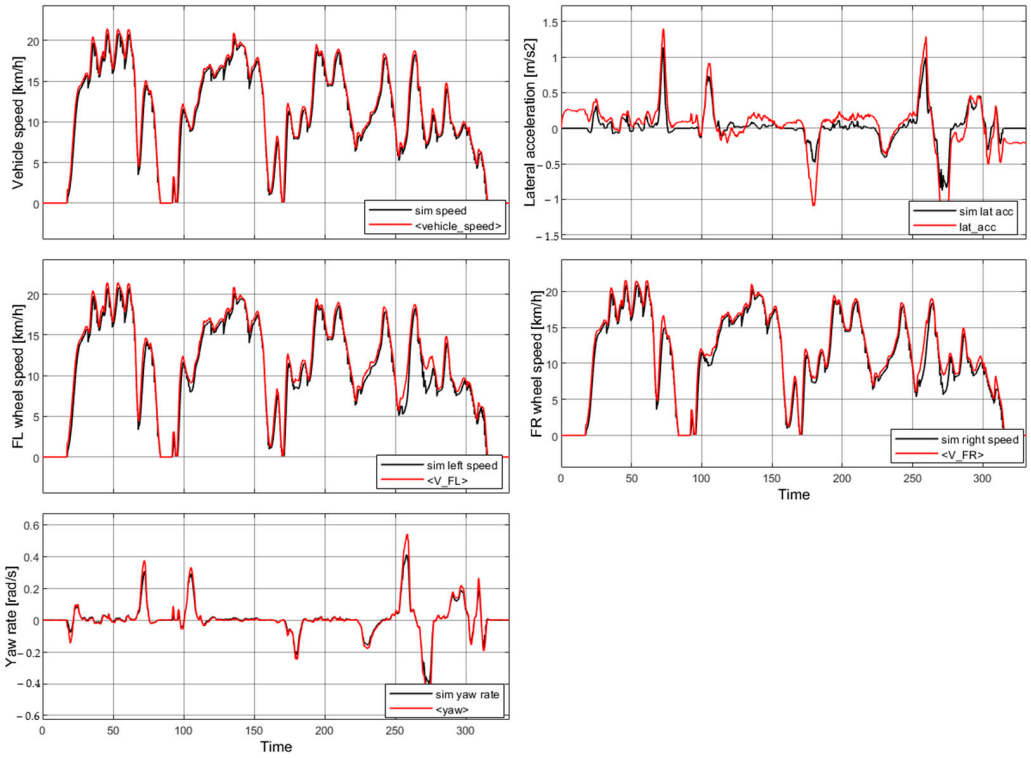


Figure 4. Virtual model real-world data correlation on step 1.

Table 1 summarizes the agreement between the simulated outputs and the CAN measurements shown in Figure 4. The coefficients of determination were 0.98334 for vehicle speed, 0.98005 and 0.97979 for the front-left and front-right wheel speeds, respectively, and 0.95696 for yaw rate. The corresponding wheel-speed RMSE values were 0.89361 and 0.90271 km/h. Lateral acceleration showed lower agreement, with an R^2 of 0.75341 and an RMSE of 0.16994 m/s^2. These results support the model's agreement with the recorded driving data but do not independently establish its accuracy under the sustained high-curvature conditions of the controller tests.

Table 1. Virtual vehicle model validation metrics for step 1.

Signal	RMSE	MAE	R^2	Pearson R
Vehicle speed (km/h)	0.8199	0.5770	0.9833	0.9959
Front-left-wheel speed (km/h)	0.8936	0.6459	0.9800	0.9952
Front-right-wheel speed (km/h)	0.9027	0.6362	0.9798	0.9948
Yaw rate (rad/s)	0.0237	0.0120	0.9569	0.9944
Lateral acceleration (m/s^2)	0.1699	0.1353	0.7534	0.9043

Figure 5 presents the second validation, including the vehicle speed, front-left- and front-right-wheel speeds, lateral acceleration, and yaw-rate outputs. As in Step 1, the measured vehicle-speed and steering-wheel-angle signals were supplied to the virtual vehicle model. The simulated outputs show agreement with the corresponding CAN measurements.

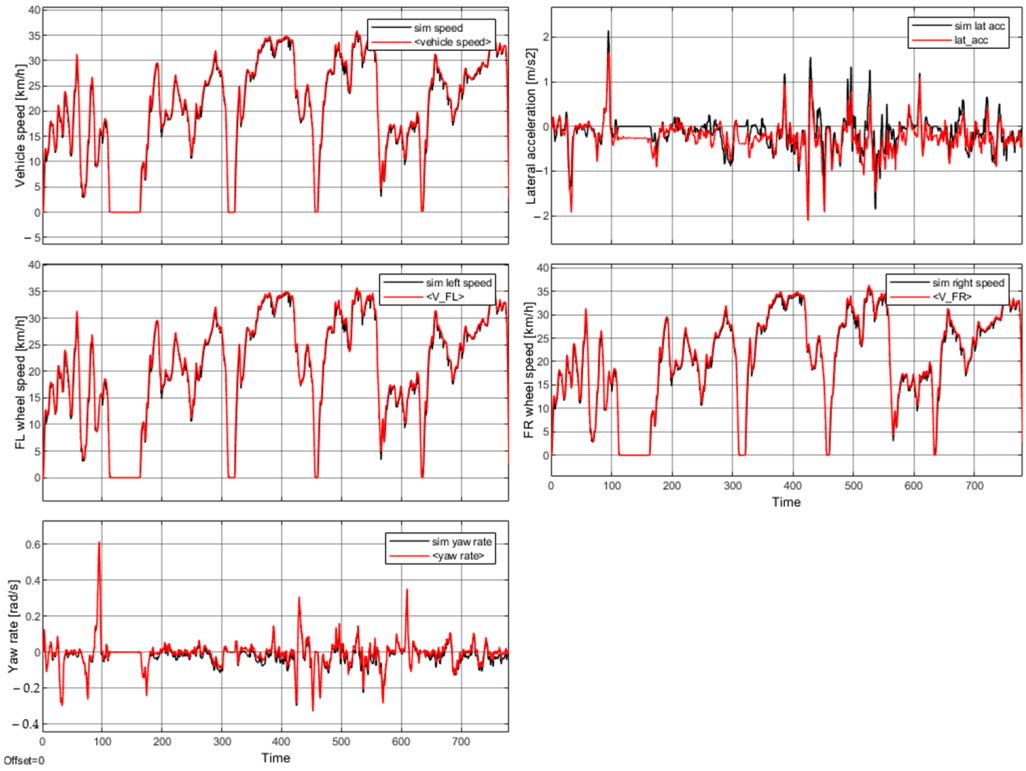


Figure 5. Virtual model real-world data correlation on step 2.

Step 2 provides an additional evaluation of the unchanged virtual vehicle model. In Table 2, the coefficients of evaluation were 0.9928 for vehicle speed, 0.9932 and 0.9921 for the front-left- and front-right-wheel speeds, and 0.9296 for yaw rate. Lateral acceleration showed weaker agreement, with an R^2 of 0.5010 and an RMSE of 0.2565 m/s^2. Thus, the second recording supports the repeatability of the speed and wheel-speed predictions and provides further evidence for the yaw-rate response, while revealing a limitation in the lateral-acceleration prediction. Because both recordings were obtained from the same vehicle under comparable conditions, this evaluation does not establish generalizability to other vehicles or substantially different driving conditions. The two recordings provide validation evidence under the observed road-driving conditions. However, the present analysis does not establish that these recordings contain sustained high-curvature maneuvers or steering operation near the limits reached in the hairpin and spiral simulations. Model accuracy under those specific conditions therefore remains unverified.

Table 2. Virtual vehicle model validation metrics for step 2.

Signal	RMSE	MAE	R^2	Pearson R
Vehicle speed (km/h)	0.8556	0.6218	0.9928	0.9983
Front-left-wheel speed (km/h)	0.8332	0.5889	0.9932	0.9982
Front-right-wheel speed (km/h)	0.8981	0.6757	0.9921	0.9982
Yaw rate (rad/s)	0.0207	0.0173	0.9296	0.9827
Lateral acceleration (m/s^2)	0.2565	0.2040	0.5010	0.8139

2.3. Model-Based Path-Tracking Set

Pure Pursuit, Model Predictive Control, and Stanley were selected as representative path-tracking controllers because they are widely used in automated vehicle applications and embody fundamentally different control principles. Lei et al. [4] identified Pure Pursuit, Stanley, and Model Predictive Control among the commonly used vehicle path-tracking methods and comparatively evaluated these approaches under the same vehicle framework. Similarly, Lee and Yim [3] included Pure Pursuit, Stanley, and Model Predictive Control within a broader comparative assessment of autonomous-vehicle path-tracking controllers, demonstrating their relevance as established benchmark approaches for evaluating lateral control performance. Pure Pursuit represents a look-ahead-based geometric approach characterized by simple implementation, low computational burden, and favorable low-speed tracking performance, whereas Stanley is an error-based geometric controller that determines steering action from heading and lateral offset errors. In contrast, Model Predictive Control represents a predictive optimization-based approach that estimates future system states and determines an optimal control sequence while allowing multiple state variables and constraints to be considered. Accordingly, the three controllers were selected not merely because of their widespread use, but because they provide representative examples of look-ahead geometric, error-based geometric, and predictive optimization-based path-tracking strategies. This selection enables a focused comparison of three established control principles on the same vehicle platform. It is not intended to cover every available path-tracking algorithm.

The test speeds were selected to represent low-speed automated path-tracking conditions associated with highly curved trajectories. Cao et al. [16] conducted full-scale autonomous path-tracking experiments using a modified BMW i3 at 5, 10, and 15 km/h, demonstrating the applicability of these speed levels to low-speed vehicle tracking tests. Li et al. [17] performed field experiments using a Wey VV6-based autonomous vehicle at speed limits of 10, 15, and 20 km/h on a route including a right-angle turn, curved sections, and lane-changing maneuvers. In their experiments, the 10 km/h condition represented the lowest tested speed and produced lower lateral and heading deviations when negotiating the high-curvature turn. Accordingly, 5 and 10 km/h were selected in the present study to represent two distinct low-speed operating conditions while remaining within speed ranges previously employed in full-scale autonomous path-tracking experiments.

2.4. Controller Design

Although Pure Pursuit, Stanley, and Model Predictive Control are primarily designed to reduce path-tracking errors, their different control principles may produce different steering command activity, lane-containment behavior, and kinematic vehicle responses, particularly under geometrically demanding maneuvers. Therefore, the controllers were evaluated not only in terms of tracking accuracy but also using safety-oriented surrogate performance measures describing lane containment, steering command activity, and kinematic vehicle-response intensity. These measures are intended to support a comparative assessment under the investigated conditions rather than to represent a complete measure of vehicle safety.

To provide a common reference-path representation and a consistent localization framework for all controllers, a Common Path Manager was implemented. The rear-axle center was used as the common vehicle reference point for route localization and tracking-error calculation. At each sampling instant, the Common Path Manager removes invalid waypoint entries, constructs the valid reference-path segments, calculates the cumulative path arc length and current path progress, and localizes the vehicle by projecting the rear-axle reference point onto candidate path segments. To prevent erroneous projection onto

geometrically close but unrelated segments, the search is restricted to an arc-length window extending 3 m behind and 20 m ahead of the previously localized path position. When geometrically equivalent candidates occur within the specified tolerance, the candidate farther along the reference path is preferred. Following the projection step, it provides the active path segment, projection ratio, current path distance, total path length, local path heading, signed cross-track error, and path-heading error. The common cross-track error is calculated from the rear-axle reference point and is defined as positive when the vehicle is located to the left of the reference-path direction. It also provides the common vehicle geometry and physical steering-angle limit used by all three controllers, while containing no controller-specific control law. Because the classical Stanley formulation defines its cross-track error at the front axle, an additional front-axle projection is performed within the Stanley controller after the common localization. This front-axle error is used only internally in the Stanley steering-law calculation, whereas the common rear-axle cross-track error provided by the Common Path Manager is used for the comparative tracking-performance evaluation of all three controllers.

Within the developed architecture, the CAN-evaluated virtual vehicle model serves as the common plant for all three controllers. At each controller update, the Common Path Manager localizes the vehicle on the same reference path and supplies shared path-progress, error, geometry, and steering-limit information. Each controller then calculates its steering command according to its own control law; Stanley additionally uses a front-axle path error required by its formulation. The resulting vehicle trajectories and responses are processed using the same evaluation procedure, including tracking errors, steering-command activity, kinematic responses, and CG-based and sampled body-based lane-containment measures. This arrangement makes the role of the common infrastructure explicit while retaining the controller-specific calculations.

Pure Pursuit was implemented using an arc-length-based target-point selection strategy regarding references [11,18]. The controller receives the current vehicle position, heading angle, longitudinal speed, and current progress along the reference path from the Common Path Manager. The nominal look-ahead distance is determined using k_d = 0.5 s and $L_{d,min}$ = 5 m [11]. For the 5 and 10 km/h test conditions considered in this study, the minimum constraint remains active and therefore L_d = 5 m in both cases.

$$L_d = max(L_{d,min}, k_d \mid V_x \mid) \tag{10}$$

In Equation (11), the target point (S_{target}) is chosen at a distance L_d from the current projection position ($S_{current}$) on the reference path.

$$S_{target} = min(S_{current} + L_d, S_{total}) \tag{11}$$

The corresponding target coordinates are obtained by linear interpolation along the reference-path segment containing S_{target}. The Euclidean distance between the rear-axle reference point and the selected target, $L_{d,actual}$, and α is the signed angular difference between the vehicle heading and the direction from the rear-axle reference point to the selected look-ahead point in Equation (12).

$$k_{cmd} = \frac{2sin(\alpha)}{L_{d,actual}} \tag{12}$$

Finally, the mean front-wheel steering command (δ_{cmd}) in Equation (13) is determined from the kinematic bicycle relation and is constrained by the same physical steering-angle limit applied to all three controllers.

$$\delta_{cmd} = tan^{-1}(WBk_{cmd}) \tag{13}$$

Model Predictive Control is a model-based predictive control approach. The controller predicts the future behavior of the vehicle over a specific prediction horizon and calculates the steering command that will minimize the defined cost function. A constrained linear Model Predictive Control based on a linearized kinematic path-error model was implemented [19]. The controller state vector was defined as $x = [e_y\ e_\psi]^T$, where e_y and e_ψ denote the cross-track and path-heading errors provided by the Common Path Manager. Under the small heading-error and steering-angle assumptions, the continuous-time error model was expressed as in Equation (14).

$$\dot{e}_y = Ve_\psi,\ \ \dot{e}_\psi = \frac{V_x}{WB}\delta_{cmd} - Vk_{ref} \tag{14}$$

The k_{ref} is the reference-path curvature. The κ_{ref} was derived directly from successive waypoint headings as a function of path arc length and interpolated over the prediction horizon. The A_d is the discrete system matrix, B_d is the steering input matrix, E_d is the road curvature effect matrix, and T_s is the sampling time. The discrete prediction model was defined in Equation (15).

$$x_{k+1} = A_d x_k + B_d \delta_{cmd} + E_d k_{ref}$$

$$A_d = \begin{bmatrix} 1 & V_x T_s \\ 0 & 1 \end{bmatrix},\ B_d = \begin{bmatrix} \frac{V_x^2 T_s^2}{2WB} \\ \frac{V_x T_s}{WB} \end{bmatrix},\ E_d = \begin{bmatrix} -\frac{V_x^2 T_s^2}{2} \\ -V_x T_s \end{bmatrix} \tag{15}$$

The Model Predictive Control parameters were established from literature-guided initial values and then examined through sensitivity analyses. The sampling time was fixed at Ts = 0.1 s [20], matching the 10 Hz sampling rate of the recorded vehicle data. The prediction and control horizons were initially set to Np = 60 [21] and Nc = 8 [22], respectively; these values provide a 6 s prediction window with eight free control moves. The initial state-error weights were qy = 1 and q_ψ = 0.5 [23]. A subsequent one-factor-at-a-time analysis varied the prediction horizon, control horizon, lateral-error weight, and heading-error weight on the hairpin and spiral paths at 10 km/h. Among the tested configurations, q_ψ = 5, with Np = 60, Nc = 8, and qy = 1, produced the lowest sampled body-based outside-lane ratio on both paths. This configuration was selected for the controller comparisons and applied unchanged at both 5 and 10 km/h. The steering-input and steering-increment weights were retained at R_δ = 0.10 and $R_{\Delta\delta}$ = 0.03, respectively. Because lateral and heading errors have different units and magnitudes, the numerical ratio of their weights should not be interpreted as a dimensionless measure of their relative importance. The selection identifies the best body-based outside-lane result within the tested configurations, rather than a global optimum.

$$J = \sum_{i=1}^{N_p} \left(q_y e_{y,i}^2 + q_\psi e_{\psi,i}^2 \right) + R_\delta \sum_{i=1}^{N_c} \delta_i^2 + R_{\Delta\delta} \sum_{i=1}^{N_c} (\Delta\delta_i)^2 \tag{16}$$

Steering commands were constrained according to Equation (17).

$$-\delta_{max} \le \delta_i \le \delta_{max}$$
$$\text{i} = 1, \ldots, \text{Nc} \tag{17}$$

The resulting quadratic programming problem was solved using the Hildreth method, and only the first element of the optimized steering sequence was applied to the vehicle model at each sampling instant, following the receding-horizon principle. The Hildreth solver was limited to 80 iterations with a convergence tolerance of 10^{-8}. After the control horizon, the final optimized steering input was held constant over the remaining prediction steps.

The hairpin scenario involves successive and sharp approximately 90° directional changes, clearly highlighting the difference between prediction horizon, heading/CTE weights, and steering-change penalty. Furthermore, 10 km/h is more challenging than 5 km/h, making insufficient horizon or poor steering smoothing more apparent. Since the desired balance between tracking accuracy and steering command activity is important, steering weights R_δ and $R_{\Delta\delta}$ were tested in this scenario.

The steering-related Model Predictive Control weights were initialized using values reported in a previous autonomous-vehicle path-following Model Predictive Control study, in which steering-input and steering-change weights of R_δ =0.10 and $R_{\Delta\delta}$ =0.03, respectively, were employed [24]. A local sensitivity analysis was subsequently performed under the 10 km/h hairpin condition by independently varying both weights to 0.5, 1, and 2 times their literature-based nominal values. The resulting nine combinations were evaluated using cross-track-error RMSE, heading-error RMSE, lateral-acceleration RMS, and steering-command-rate RMS. The analysis showed that changes in the steering penalties produced only limited variations in cross-track error, whereas clearer differences were observed in heading error, lateral-acceleration response, and steering-command activity. Increasing the steering penalties generally reduced lateral-response and steering-command-activity measures, although this was accompanied by a slight increase in lateral tracking error for the highest penalty combinations. This analysis was performed around the initial state-error-weight configuration with qy = 1 and qψ = 0.5. The literature-based steering-weight combination R_δ = 0.10 and $R_{\Delta\delta}$ = 0.03 was retained for the subsequent horizon and tracking-weight analysis and for the final controller comparisons. The sensitivity results are presented in Table 3.

Table 3. Steering weights sensitivity check results.

R_δ	$R_{\Delta\delta}$	CTE_{RMSE} (m)	$Heading_{RMSE}$ (deg)	$a_{y,RMS}$ (m/s^2)	$\dot{\delta}_{RMS}$(deg/s)
0.05	0.015	0.39011	15.903	0.9679	1062.32
0.05	0.030	0.38993	15.895	0.9652	1074.91
0.05	0.060	0.38919	15.877	0.9581	933.72
0.10	0.015	0.39071	15.853	0.9494	990.07
0.10	0.030	0.39007	15.842	0.9468	976.59
0.10	0.060	0.39009	15.898	0.9426	903.68
0.20	0.015	0.39249	15.767	0.9232	802.23
0.20	0.030	0.39262	15.767	0.9226	828.99
0.20	0.060	0.39284	15.764	0.9208	834.74

Pure Pursuit and Stanley were evaluated with fixed parameters selected from prior studies employing comparable path-tracking formulations and low-speed operating conditions. These parameters were retained across all test scenarios. For Model Predictive Control, the steering-input and steering-increment weights were retained at their literature-guided values, whereas the heading-error weight was selected through the additional sensitivity analysis based on the sampled body-based outside-lane ratio. The final Model Predictive Control configuration was Np = 60, Nc = 8, qy = 1, qψ = 5, R_δ = 0.10 and $R_{\Delta\delta}$ = 0.03. Because an identical tuning procedure was not applied to all three controllers, the results should not be interpreted as a ranking of their best attainable performance.

To complement the steering-weight sensitivity analysis in Table 3, an additional one-factor-at-a-time analysis was performed for the Model Predictive Control prediction horizon, control horizon, and tracking-error weights. The prediction horizon was varied over Np = {10, 30, 60, 90}, the control horizon over Nc = {2, 8, 16}, the lateral-error weight over qy = {0.1, 1, 10}, and the heading-error weight over qψ = {0.05, 0.5, 5}. Each parameter was varied independently while the remaining parameters retained their initial nominal values. The ten parameter configurations were evaluated separately on the hairpin and spiral paths at 10 km/h, resulting in 20 scenario-specific cases in total. The fixed sampling interval was Ts = 0.1 s. Sensitivity was assessed using cross-track-error RMSE, heading-error RMSE, steering-wheel command-rate RMS, and the sampled body-based outside-lane ratio, B_{out}. The analysis was used to select the configuration with the lowest B_{out} among the tested cases and does not represent a global or scenario-specific optimization. Table 4 presents the results of the additional sensitivity analysis.

Table 4. Model Predictive Control horizon and tracking-weight sensitivity on the hairpin and spiral paths at 10 km/h.

Scenario	Np	Nc	qy	qψ	CTE RMSE (m)	Heading RMSE	Steering-Wheel Command-Rate RMS (°/s)	B_{out} (%)
Hairpin	60	8	1	0.5	0.3901	15.842	976.59	43.509
Hairpin	10	8	1	0.5	0.9414	18.965	1686.6	43.795
Hairpin	30	8	1	0.5	0.3759	15.749	759.95	43.224
Hairpin	90	8	1	0.5	0.3671	15.612	1099.8	44.650
Hairpin	60	2	1	0.5	0.6338	16.622	982.47	58.631
Hairpin	60	16	1	0.5	0.3929	15.945	873.67	43.652
Hairpin	60	8	0.1	0.5	0.3962	15.62	483.6	43.509
Hairpin	60	8	10	0.5	0.3850	16.003	1316.3	44.508
Hairpin	60	8	1	0.05	0.3881	15.888	998.47	44.080
Hairpin	60	8	1	5	0.4023	15.778	881.9	43.081
Spiral	60	8	1	0.5	0.5845	16.498	1111.6	35.742
Spiral	10	8	1	0.5	1.1778	21.691	1029.2	44.12
Spiral	30	8	1	0.5	0.6259	16.392	986.02	38.125
Spiral	90	8	1	0.5	0.6308	17.843	1492.3	47.271
Spiral	60	2	1	0.5	0.7911	17.837	1321.8	56.879
Spiral	60	16	1	0.5	0.6389	17.024	1162.9	38.97
Spiral	60	8	0.1	0.5	0.6176	16.03	603.9	35.819
Spiral	60	8	10	0.5	0.5909	16.455	1994.2	36.741
Spiral	60	8	1	0.05	0.5866	16.61	1190.8	36.741
Spiral	60	8	1	5	0.5969	16.202	1116.5	33.513

The Stanley controller determines the steering command from two primary tracking quantities: the front-axle cross-track error and the heading error relative to the local reference-path direction. In this study, the classical front-axle Stanley formulation was employed using the classical front-axle error formulation regarding literature [5,25]. Since the common vehicle reference point was located at the rear-axle center, the front-axle coordinates were first calculated as in Equation (18).

$$X_f = X + WBcos\psi,\ Y_f = Y + WBsin\psi \tag{18}$$

The front-axle center was then locally projected onto the common reference path, and the heading of the corresponding path segment was used as the Stanley reference heading.

The signed front-axle cross-track error was calculated as in Equation (19). X_p and Y_p denote the projected reference point.

$$e_f = -(X_f - X_p)sin\psi_{ref} + (Y_f - Y_p)cos\psi_{ref} \tag{19}$$

The heading difference ($\Delta\psi$) is in Equation (20).

$$\Delta\psi = \psi_{ref} - \psi \tag{20}$$

The heading correction used in the Stanley controller is in Equation (21).

$$e_{\psi,s} = \begin{cases} \Delta\psi - 2\pi, \ \Delta\psi > \pi \\ \Delta\psi + 2\pi, \ \Delta\psi < -\pi \\ \Delta\psi, \ -\pi \leq \Delta\psi \leq \pi \end{cases} \tag{21}$$

To avoid excessive cross-track correction at low vehicle speeds, a velocity-softening term was included. The cross-track correction was therefore calculated as in Equation (22).

$$\delta_e = tan^{-1}\left(\frac{k_s e_f}{|V| + v_s}\right) \tag{22}$$

where $k_S = 1\ s^{-1}$ [26] is the Stanley gain and $v_s = 1$ m/s [27] is the softening speed. Based on the sign convention adopted in this study, positive cross-track error indicates that the front axle is located to the left of the reference path. Therefore, the final δ_{cmd} was obtained as in Equation (23).

$$\delta_{cmd} = e_{\psi,s} - \delta_e \tag{23}$$

Finally, the command was constrained by the same physical δ_{cmd} limit used for the Pure Pursuit and Model Predictive Control controllers as in Equation (24).

$$-\delta_{max} \leq \delta_{cmd} \leq \delta_{max} \tag{24}$$

The comparison uses fixed controller configurations rather than parameter sets obtained through a common optimization procedure. For Pure Pursuit, the minimum look-ahead distance of 5 m is active at both test speeds, providing the same nominal preview distance. For Stanley, the selected gain and velocity-softening term determine the cross-track correction and moderate its magnitude at low speeds. For Model Predictive Control, the sampling time matches the CAN acquisition interval, while the prediction and control horizons define the preview window and the number of free control moves. The steering-input and steering-increment penalties were retained at their literature-guided values, and the heading-error weight was selected from the tested sensitivity configurations using the sampled body-based outside-lane ratio. All final controller parameters were then kept unchanged across the comparison scenarios. Accordingly, the results characterize the selected implementations under common test conditions and do not establish the best achievable performance of each controller family. The absence of a uniform tuning procedure remains a limitation of the comparison.

Figure 6 shows a comprehensive Simulink model designed to simulate the physical movements and path-following performance of an electric and autonomous vehicle in a virtual environment. Essentially, it incorporates longitudinal vehicle dynamics together with a kinematic steering and planar-motion representation for path tracking. In the upper left of the model is a controller that mimics a real driver's reactions. This structure continuously compares the vehicle's current actual speed to a given target speed, determining how much throttle or brake is needed. These commands are transmitted to the battery, electric motor,

and braking systems. The torque produced by the motor, along with challenging forces such as friction and air resistance, is calculated and combined in the transmission block to obtain the vehicle's instantaneous acceleration and linear velocity. The middle and upper right sections of the image calculate the simulated vehicle position in the global X−Y coordinate system on a 2D plane in real time, using the vehicle speed, steering geometry, and calculated yaw response. This allows for continuous calculation of the simulated vehicle position and its relation to the reference path on the map and its deviation from its intended course. At the bottom of the model are autonomous driving algorithms. The Common Path Manager analyzes the plotted route and curves, preparing the information needed by the control algorithms. The data from the Common Path Manager is fed to Pure Pursuit, which is based on geometric calculations; the Model Predictive Control algorithm, which predicts the vehicle's future movements and makes optimal decisions; and the Stanley controller, which employs a front-axle tracking-error formulation.

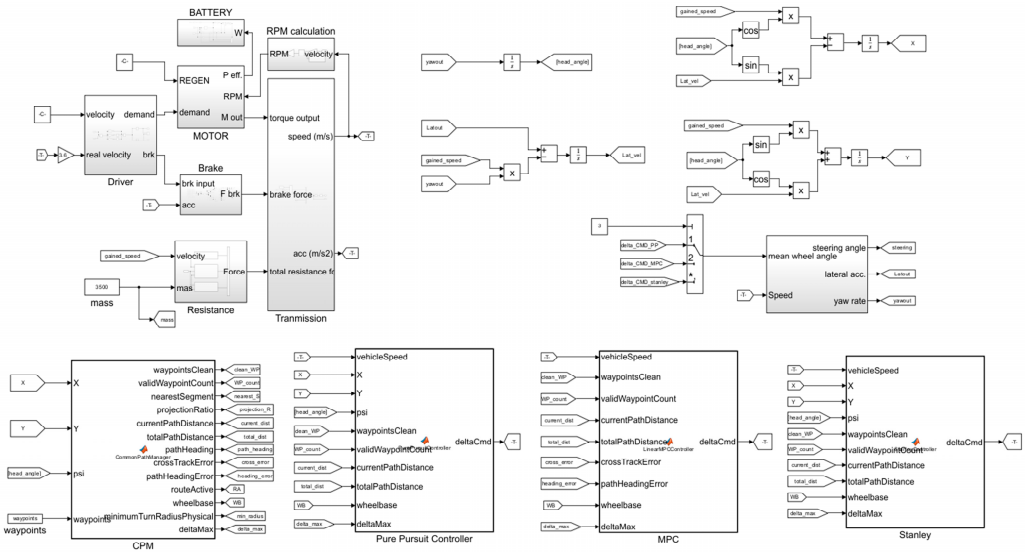


Figure 6. Path-tracking-ready virtual vehicle model.

Figure 6 shows the linear and lateral theoretical calculations as well as auxiliary metrics. Head angle, lateral velocity, and X and Y positions are outputs of the integrated model created for controller comparison. In Equation (25), head angle (φ) in radians is determined by integrating the yaw-rate value.

$$\varphi(t) = \varphi(t_0) + \int_{t_0}^{t} r dt \tag{25}$$

In Equation (26), the lateral velocity is the velocity of the vehicle along its lateral axis relative to its instantaneous position, expressed in m/s. In the equation, V_y is the lateral velocity, and a_y is the lateral acceleration.

$$V_y = \int_{t_0}^{t} (a_y - V_x r) dt \tag{26}$$

Equation (27) calculates the vehicle's instantaneous position in meters along the horizontal (X) and vertical (Y) axes.

$$\begin{aligned} X(dt) &= X(t_0) + \int_{t_0}^{t} \left[V_x \cos(\varphi) - V_y \sin(\varphi)\right] dt \\ Y(dt) &= Y(t_0) + \int_{t_0}^{t} \left[V_x sin(\varphi) + V_y cos(\varphi)\right] dt \end{aligned} \tag{27}$$

2.5. Safety-Oriented Surrogate Performance Measures

To measure the lane-keeping performance of autonomous vehicles, it is generally necessary to examine how much the vehicle deviates from its lane, its steering movements, and its kinematic vehicle responses. In the literature [6,8,28], calculating the mean error is a common method for assessing driving precision. In addition to tracking-error measures, steering-command activity, yaw rate, and lateral acceleration provide complementary information on the controller-induced kinematic vehicle response. From a safety perspective, keeping the vehicle within lane boundaries by the control algorithms is considered one of the most fundamental requirements. In this study, instead of focusing on a single parameter, metrics such as the cross-track error (CTE), Root Mean Square Error (RMSE), heading-error RMSE, outside-lane ratio, steering-command-rate RMS, maximum lateral acceleration, lateral-acceleration RMS, minimum lane margin, and yaw-rate RMS are evaluated together. In this study, the term "safety-oriented" refers to the joint consideration of tracking errors, CG-based and body-based lane-boundary violations, steering-command activity, and kinematic-response measures as safety-related performance indicators. These quantities describe selected aspects of controller behavior under the prescribed simulation conditions; they do not directly quantify collision risk or establish overall vehicle safety.

The CTE_{RMSE} value in Equation (28) quantifies the root-mean-square lateral deviation of the common rear-axle reference point from the reference path.

$$CTE_{RMSE} = \sqrt{\frac{1}{T}\int_{t_0}^{t_f} e_y^2(t)dt} \tag{28}$$

$$T = t_f - t_0$$

The heading-error RMSE (φ_{RMSE}) in Equation (29) indicates how much the vehicle's orientation deviates from the path alignment. This metric is particularly important when entering and exiting curves. The $e_{\varphi,deg}$ is the heading error in degrees.

$$\varphi_{RMSE} = \sqrt{\frac{1}{T}\int_{t_0}^{t_f} e_{\varphi,deg}^2(t)dt} \tag{29}$$

The steering-command-rate RMS in Equation (30) quantifies changes in the steering-wheel angle command generated by each controller. The recorded command is converted from radians to degrees and sampled on a uniform time grid with Ts = 0.1 s using the previous recorded value at each sampling instant. Successive command differences are divided by Ts, and their root-mean-square value is calculated over the evaluation interval without additional smoothing. The reported metric is expressed in degrees per second and refers to the steering-wheel command rather than the front-road-wheel steering angle. The model constrains steering-command magnitude but does not include steering-actuator dynamics or steering-rate saturation. Accordingly, this metric describes simulated command activity and does not establish physically achievable actuator motion. Its value depends on the

sampling interval and numerical evaluation method; the finite-difference calculation alone does not exclude contributions from solver behavior or quantization.

$$\dot{\delta}_{RMS} = \sqrt{\frac{1}{N-1}\sum_{k=1}^{N-1}\left(\frac{\dot{\delta}_{k+1}-\dot{\delta}_k}{T_s}\right)^2} \tag{30}$$

In Equation (31), lateral acceleration RMS ($a_{y,RMS}$) quantifies the root-mean-square magnitude of the kinematic lateral-acceleration response over the maneuver. In this respect, it distinguishes the intensity of lateral movement and, indirectly, the rotational-response intensity. It shows the lateral response throughout the entire drive, not just a single maximum value.

$$a_{y,RMS} = \sqrt{\frac{1}{T}\int_{t_0}^{t_f} a_y^2(t)dt} \tag{31}$$

The yaw-rate RMS (r_{RMS}) in Equation (32) considers the yaw rate values generated throughout the entire drive and reveals the overall behavior. It represents how intensely the vehicle's orientation changes throughout the maneuver.

$$r_{RMS} = \sqrt{\frac{1}{T}\int_{t_0}^{t_f} r^2(t)dt} \tag{32}$$

In Equation (33), the outside-lane ratio (R_{out}) is the ratio of instances where the CG goes outside the lane and is a safety-oriented surrogate measure of lane-containment violation prevalence. At each sampling point, it is checked whether the vehicle's CG point is inside or outside the lane corridor. The $I_{out}(i)$ display function is the R_{out} outside-lane ratio.

$$\begin{aligned} I_{out}(i) &= \begin{cases} 1, & CG_i \text{isoutofline} \\ 0, & CG_i \text{isinline} \end{cases} \\ R_{out} &= \frac{100}{N}\sum_{i=1}^{N} I_{out}(i) \end{aligned} \tag{33}$$

The maximum absolute lateral acceleration, defined in Equation (34), represents the peak magnitude of the lateral-acceleration response over the evaluation interval from t_0 to t_f.

$$a_{y,max} = \max_{t\in[t_0,t_f]} \left|a_y(t)\right| \tag{34}$$

In each scenario run, the vehicle body was modeled as a rectangle positioned at the center of gravity (CG) and rotated by the absolute heading angle. The rectangle representing the vehicle has an approximate length of 6 m and a width of 2 m. The distances from the CG to the front and rear wheel centers are approximately 1.8 m. The portion of the vehicle body rectangle falling within the 3.75 m wide lane corridor was subtracted. If the remaining area exceeded a tolerance of 10^{-8} m^2, that sample was classified as "body partially outside the lane." Merely touching the boundary did not constitute a violation, as it did not generate an area. In Equation (35), Nb represents the number of samples where the body is partially outside, while N_T represents the total number of data samples evaluated in that scenario; B_{out} denotes the ratio of the body being outside the lane.

$$B_{out} = \frac{N_b}{N_T}100 \tag{35}$$

The minimum lane margin indicates the closest signed distance of the vehicle's CG to the lane boundary over the entire maneuver. At each sample, the Euclidean distance

between the vehicle CG and the nearest boundary of the lane corridor is calculated. In this study, the lane width was set to 3.75 m. A signed lane margin, Mi, is then assigned according to the CG location: Mi > 0 when the CG is inside the lane corridor, Mi = 0 when it lies on the boundary, and Mi < 0 when it is outside the lane corridor. A positive M_{min} indicates that the CG remained within the lane throughout the maneuver, whereas a negative value indicates a lane-boundary violation, with a larger negative magnitude corresponding to a more severe excursion.

$$d_i = \min |CG - q|$$

$$M_i = \begin{cases} +d_i, \text{ CG inside} \\ 0, \text{ CG on boundary} \\ -d_i, \text{ CG outside} \end{cases} \quad (36)$$

$$M_{min} = \min(M_i)$$

Two reference-path profiles, termed hairpin and spiral, were used to evaluate controller behavior under challenging geometric conditions, as shown in Figure 7. Both references are piecewise-linear paths comprising straight segments connected by approximately 90° heading changes. The hairpin contains successive turns, whereas the spiral progresses inward, producing nested and spatially adjacent path segments within a constant-width lane corridor. These configurations test tracking accuracy, steering-command activity, and CG-based lane keeping during repeated changes in reference heading. They are intended as idealized geometric stress tests rather than physically feasible trajectories for exact tracking. A vehicle with a finite turning radius cannot track their vertices without deviation; therefore, the measured errors reflect both controller behavior and reference-path infeasibility. The resulting controller rankings should consequently be interpreted within these test conditions and should not be generalized to curvature-continuous paths without additional evaluation. Vehicle parameters, lane width, steering-angle limits, and controller update times were identical across the controller comparisons. Both scenarios were evaluated at target speeds of 5 and 10 km/h.

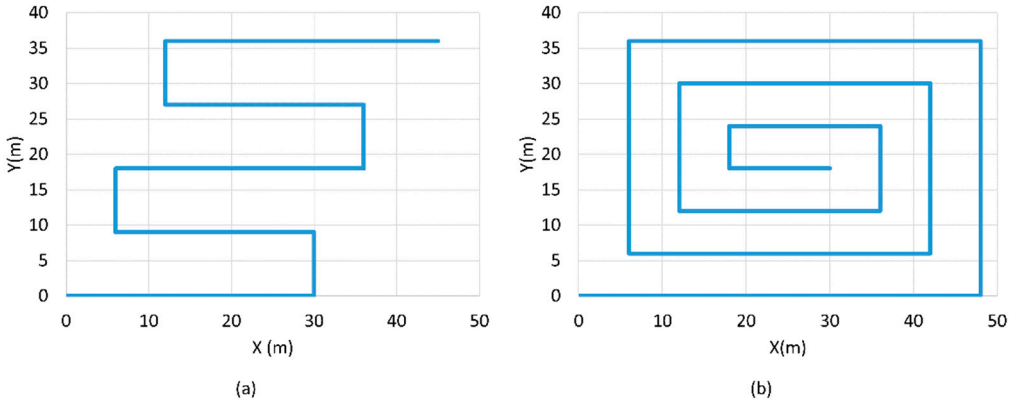


Figure 7. Path scenarios: (**a**) hairpin, (**b**) spiral.

3. Results

This section presents the comparative performance results of Pure Pursuit, Stanley, and Model Predictive Control algorithms in two different driving scenarios. Evaluations were conducted under real data-validated vehicle models, roadmap infrastructure, and operating limits, at constant speeds of 5 and 10 km/h on both spiral and hairpin routes. The controllers' performance was compared in a multidimensional way based on parameters such as CTE_{RMSE}, heading-error RMSE, steering-command-rate RMS, maximum and RMS

lateral acceleration, yaw-rate RMS, outside-lane ratio, minimum lane margin, and outside-lane ratio of CG and vehicle body. The obtained numerical data are summarized in Tables 5–8, and graphs showing the path-tracking characteristics of the controllers are presented in Figures 8 and 9.

Table 5. Path-tracking performance results on the hairpin scenario.

	Vx (km/h)	CTE_{RMSE} (m)	φ_{RMSE} (°)	$\dot{\delta}_{RMS}$ (deg/s)	$a_{y,max}$ (m/s^2)	$a_{y,RMS}$ (m/s^2)	r_{RMS} (rad/s)	M_{min} (m)
Pure Pursuit	5	0.525	15.9	128.19	0.386	0.219	0.160	0.748
Model Predictive Control	5	0.342	15.9	576.86	0.386	0.236	0.172	0.934
Stanley	5	0.510	15.9	442.24	0.386	0.226	0.165	0.596
Pure Pursuit	10	0.503	15.3	247.86	1.565	0.857	0.311	0.767
Model Predictive Control	10	0.4023	15.8	881.9	1.5651	0.925	0.335	0.732
Stanley	10	0.617	15.5	635.67	1.565	0.874	0.316	0.540

Table 6. Outside ratios for hairpin scenario.

	Vx (km/h)	R_{out} (%)	B_{out} (%)
Pure Pursuit	5	0	48.271
Model Predictive Control	5	0	37.048
Stanley	5	0	43.659
Pure Pursuit	10	0	51.783
Model Predictive Control	10	0	43.081
Stanley	10	0	53.352

Table 7. Path-tracking performance results on the spiral scenario.

	Vx (km/h)	CTE_{RMSE} (m)	φ_{RMSE} (°)	$\dot{\delta}_{RMS}$ (deg/s)	$a_{y,max}$ (m/s^2)	$a_{y,RMS}$ (m/s^2)	r_{RMS} (rad/s)	M_{min} (m)
Pure Pursuit	5	0.712	17.843	144.11	0.386	0.191	0.139	−1.123
Model Predictive Control	5	0.595	15.627	683.42	0.386	0.223	0.163	−1.109
Stanley	5	0.739	15.614	506.51	0.386	0.203	0.148	−1.116
Pure Pursuit	10	0.704	19.274	285.84	1.565	0.761	0.276	−1.091
Model Predictive Control	10	0.597	16.202	1111.6	1.5651	0.836	0.303	−1.083
Stanley	10	0.785	15.308	710.04	1.565	0.787	0.285	−1.112

Table 8. Outside ratios for spiral scenario.

	Vx (km/h)	R_{out} (%)	B_{out} (%)
Pure Pursuit	5	2.879	41.383
Model Predictive Control	5	2.359	36.505
Stanley	5	2.839	39.424
Pure Pursuit	10	2.767	44.197
Model Predictive Control	10	2.383	33.513
Stanley	10	2.844	46.964

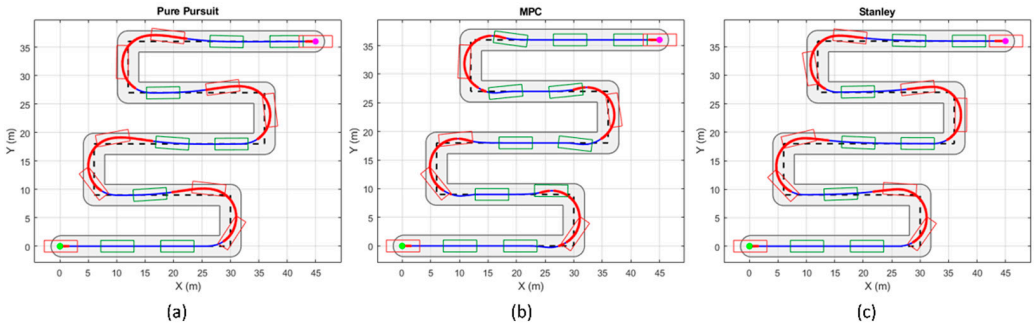


Figure 8. Path-tracking behaviors on the hairpin scenario: (**a**) pure pursuit, (**b**) Model Predictive Control, (**c**) Stanley.

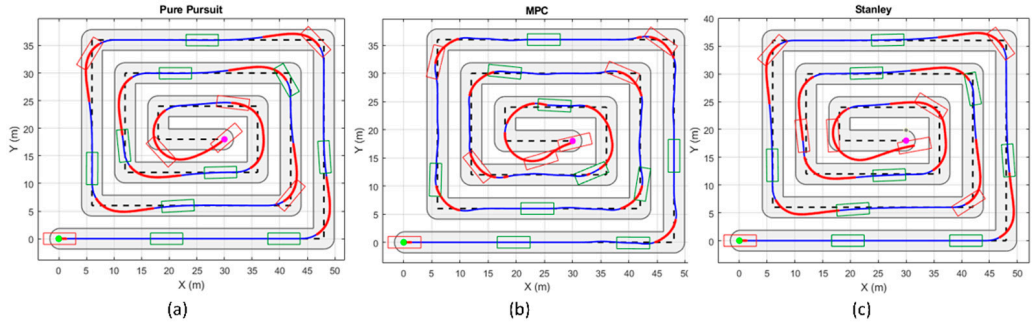


Figure 9. Path-tracking behavior on the spiral scenario: (**a**) pure pursuit, (**b**) Model Predictive Control, (**c**) Stanley.

3.1. Control Performance Results on the Hairpin Scenario

According to Table 5, in the hairpin scenario, Model Predictive Control achieved the lowest cross-track-error RMSE at both speeds. At 5 km/h, Model Predictive Control also produced the largest minimum lane margin, whereas Pure Pursuit produced the lowest steering-command-rate RMS, lateral-acceleration RMS, and yaw-rate RMS values. At 10 km/h, Pure Pursuit retained the largest minimum lane margin and the lowest steering-command-rate RMS, lateral-acceleration RMS, and yaw-rate RMS values. For all three controllers, the vehicle CG remained within the lane boundaries throughout the hairpin scenario, yielding a 0% CG-based outside-lane ratio. However, Table 6 shows that the vehicle body was partially outside the modeled lane corridor in a substantial proportion of evaluated samples. Detailed tracking behavior can be seen in Figure 8.

Table 6 shows that the CG-based outside-lane ratio was 0% for every controller at both speeds. The body-based assessment gives a different result: the body was partially outside the lane in 37.048–48.271% of evaluated samples at 5 km/h and 43.081–53.352% at 10 km/h. Model Predictive Control had the lowest body outside-lane ratio at both speeds, with values of 37.048% and 43.081%, respectively. Thus, the absence of CG boundary crossings in the hairpin tests did not imply full-body containment within the modeled lane corridor.

3.2. Control Performance Results on the Spiral Scenario

In the spiral scenario, the differences between the controllers become apparent. MPC achieved the lowest cross-track-error RMSE and the lowest body-based outside-lane ratio at both speeds, whereas Stanley achieved the lowest heading-error RMSE. Pure Pursuit exhibited the lowest steering-command-rate RMS, lateral-acceleration RMS, and yaw-rate RMS values. All three controllers produced nonzero CG-based outside-lane ratios and negative minimum CG-to-boundary margins, indicating that the vehicle CG crossed the lane boundaries during the spiral scenario. Detailed tracking behavior is shown in Figure 9, and the numerical results are presented in Table 7.

Table 8 further shows that body-based outside-lane ratios were substantially higher than the corresponding CG-based ratios in the spiral scenario. At 5 km/h, the CG-based ratios ranged from 2.359% to 2.879%, whereas the body-based ratios ranged from 36.505% to 41.383%. At 10 km/h, the corresponding ranges were 2.383–2.844% and 33.513–46.964%. MPC produced the lowest body-based ratio at both speeds, although its body was still partially outside the modeled lane corridor in 36.505% and 33.513% of evaluated samples, respectively.

4. Discussion

The results show that controller performance depends on the performance metric considered. Model Predictive Control excels in tracking accuracy, achieving the lowest CTE_{RMSE} values in both hairpin and spiral scenarios, while Pure Pursuit consistently maintained the lowest RMS values for steering-command-rate RMS, lateral acceleration, and yaw rate. Stanley, on the other hand, presented the lowest heading RMSE in the spiral scenario.

The high steering-wheel command-rate RMS values obtained with Model Predictive Control require careful interpretation. The present model constrains the steering-command magnitude but does not represent steering-actuator dynamics or impose a steering-rate limit. Consequently, the reported metric characterizes command variation within the simulation and does not establish that an actual steering system could reproduce these commands. Although the Model Predictive Control cost function penalizes changes in steering input, this penalty does not enforce actuator feasibility. In a physical implementation, finite actuator bandwidth and steering-rate saturation would limit how closely the applied steering angle follows rapid command changes, potentially affecting tracking errors, CG-based lane margins, and the relative performance of the controllers. Therefore, Model Predictive Control's lower cross-track error should be interpreted within the present idealized steering configuration. Quantifying the effect of actuator limitations requires additional simulations using an actuator model and vehicle-specific steering-rate limits.

The reference-path geometry also limits the interpretation of these comparisons. Both the hairpin and spiral references contain approximately 90° heading discontinuities that cannot be tracked exactly by a vehicle with a finite turning radius. Consequently, the tracking errors and steering-command activity reflect both controller behavior and reference-path infeasibility. Using identical paths for all controllers does not eliminate the potentially different effects of this geometry on each control strategy. The reported rankings therefore apply to the investigated geometric stress tests; their applicability to curvature-continuous paths has not been established.

For Pure Pursuit, the minimum look-ahead constraint Ld,min = 5 m is active at both 5 and 10 km/h because the speed-dependent term kd*|Vx| remains below this value. Consequently, Pure Pursuit uses the same geometric preview distance at both test speeds. This fixed-preview configuration provides a consistent, literature-guided controller parameterization across the scenarios, but it also limits the interpretation of the difference between the two speeds: the comparison does not represent a fully speed-adaptive Pure Pursuit implementation. A smaller minimum look-ahead distance could produce a different balance between tracking accuracy and steering-command activity. Therefore, the reported results characterize the specified fixed-preview Pure Pursuit configuration, while a systematic speed-scaled look-ahead study remains a subject for future work.

These findings are consistent with comparative studies in the literature. For example, Hossain et al. [12], in their research comparing Pure Pursuit, Stanley, Linear–Quadratic Regulator, and Model Predictive Control on sharp curved trajectories, reported that Model Predictive Control yielded lower average lateral error compared to Pure Pursuit and Stanley.

This finding is consistent with the strong tracking accuracy exhibited by Model Predictive Control in our current study. On the other hand, Rumetshofer et al. [10] showed that Pure Pursuit reduced steering effort by accepting some lateral error, while Stanley tightened tracking at the cost of higher steering load. Jung [11] made a similar observation, stating that the look-ahead distance in Pure Pursuit directly balances smooth steering movements with tracking accuracy, while Stanley's responses become more sensitive, especially at points where geometric transitions become sharper. All these observations are consistent with the controller characteristics revealed in our hairpin and spiral tests.

The CG-based outside-lane ratio provides information that the rear-axle cross-track error alone cannot capture. In the hairpin scenario, the vehicle CG remained within the lane boundaries for all three controllers, although the minimum CG-to-boundary margins differed. In the spiral scenario, the CG crossed the lane boundaries for all three controllers. At 5 km/h, MPC achieved the lowest CG-based outside-lane ratio, whereas Stanley yielded the least-negative minimum margin. At 10 km/h, MPC yielded both the lowest CG-based outside-lane ratio and the least-negative minimum margin. The outside-lane ratio describes the proportion of evaluated samples with the CG outside the lane, while the minimum margin describes the largest CG excursion beyond a boundary. Both metrics are therefore useful, but neither accounts for the full vehicle footprint or its swept envelope during cornering.

The similar minimum CG-to-boundary margins in the spiral scenario should be distinguished from the differences in the CG-based outside-lane ratio. The minimum margin represents the most severe excursion during a maneuver, whereas the outside-lane ratio represents the proportion of evaluated samples for which the CG is outside the lane. Controllers can therefore produce similar worst-case excursions while differing in the duration and frequency of boundary violations. The shared inward-tightening path geometry and steering-angle constraint offer a plausible explanation for the minimum margins clustering around -1.1 m. However, these aggregate metrics alone do not establish that the minimum margins occurred at the same path location or resulted from the same steering behavior.

The nearly identical maximum lateral accelerations are consistent with the kinematic relation in Equation 8, which links lateral acceleration to vehicle speed and turning radius. At a given speed, controllers reaching similar minimum turning radii will produce similar peak lateral accelerations. The common steering-angle limit provides a possible mechanism for this behavior, although confirming steering saturation requires examination of the steering-command histories. The approximately fourfold increase in peak lateral acceleration between 5 and 10 km/h is also consistent with the squared-speed dependence of Equation 8. In contrast, lateral-acceleration RMS depends on the response over the entire maneuver and can therefore distinguish controllers that attain similar peaks but differ in the duration and distribution of their turning responses.

The controller evaluations were performed as deterministic single simulations under identical initial conditions, vehicle parameters, reference paths, sampling time, and steering constraints. No random disturbances, sensor noise, initial-state perturbations, or timing jitter were introduced. Therefore, the reported metrics are point estimates for the investigated configurations and do not provide confidence intervals or a statistical assessment of controller robustness. The two CAN recordings support virtual-model validation but do not constitute repeated controller experiments. Future work should include repeated simulations with perturbed initial conditions, measurement noise, timing variations, and model-parameter uncertainty.

In general, the findings directly support the multidimensional evaluation approach discussed by Artuñedo et al. [1]. The researchers emphasized that the character of a

controller cannot be fully determined by looking only at lateral or angular tracking errors. Control inputs and the vehicle's dynamic responses to these inputs must also be taken into account. Similarly, Lee and Yim [3] showed that traditional lateral and heading-error metrics alone are insufficient to reflect the instantaneous response capability of the controller. Indeed, the results obtained in this study clearly demonstrate that no controller was superior across all evaluated metrics in every aspect. Model Predictive Control stood out with its lateral tracking accuracy and lane-containment performance. Pure Pursuit provided lower steering-command activity and lower kinematic-response intensity by reducing steering effort. Stanley, on the other hand, managed to maintain directional alignment more strongly, especially in the spiral scenario.

5. Conclusions

This study compared Pure Pursuit, Stanley, and Model Predictive Control (MPC) on a common virtual vehicle platform evaluated against two separate CAN recordings from the same vehicle without recalibration. The Common Path Manager supplied consistent reference-path information, vehicle geometry, and steering constraints. Controller behavior was examined at 5 and 10 km/h on hairpin and spiral paths using tracking, steering-command, kinematic-response, and lane-containment measures.

The results show why tracking error alone does not characterize controller performance under the investigated conditions. MPC achieved the lowest cross-track-error RMSE in both scenarios, while Pure Pursuit generally produced the lowest steering-command-rate, lateral-acceleration, and yaw-rate RMS values. Stanley achieved the lowest heading-error RMSE in the spiral scenario. The body-based assessment revealed a further distinction: although every controller maintained its center of gravity within the hairpin lane, the vehicle body was partially outside the modeled corridor in 37.048–53.352% of evaluated samples. Thus, center-of-gravity containment did not establish full-body containment. Assessing vehicle-body position alongside tracking accuracy, steering activity, and kinematic response provides a more complete description of these simulations.

Both validation recordings came from one vehicle, and lateral-acceleration agreement was weaker than that of the other evaluated signals, particularly in the second recording. The controller comparison used specified parameter configurations without a uniform optimization procedure and a kinematic vehicle model that does not represent tire slip or load transfer. The body-containment measure evaluated sampled vehicle positions rather than the area swept between samples. These factors limit the transfer of the findings to other vehicles and operating conditions.

The steering model constrains command magnitude but omits actuator dynamics and steering-rate limits. The reported steering-wheel command-rate RMS therefore characterizes simulated command activity and does not establish physical actuator feasibility. Actuator lag and rate saturation could alter tracking errors, CG-based lane margins, and controller rankings. Furthermore, the piecewise-linear reference paths are idealized geometric stress tests, and the findings should not be generalized to curvature-continuous trajectories without additional evaluation.

Future work should evaluate curvature-continuous reference paths, incorporate vehicle-specific steering-actuator dynamics and rate limits, and extend the body-containment measure to the swept vehicle envelope. Validation using other vehicles and driving conditions, followed by physical controller tests and a broader, consistent parameter-tuning study, is needed to assess whether the observed trade-offs persist beyond the present simulation setting. The CAN recordings do not independently establish model accuracy during sustained high-curvature, near-limit steering maneuvers.

Funding: This research received no external funding.

Institutional Review Board Statement: Not applicable.

Informed Consent Statement: Not applicable.

Data Availability Statement: The CAN data are not publicly available because of applicable commercial-confidentiality restrictions. Derived validation results and simulation outputs can be provided by the corresponding author upon reasonable request, subject to these restrictions.

Conflicts of Interest: The author declares no conflicts of interest.

References

1. Artuñedo, A.; Moreno-Gonzalez, M.; Villagra, J. Lateral Control for Autonomous Vehicles: A Comparative Evaluation. *Annu. Rev. Control* **2024**, *57*, 100910. [CrossRef]
2. Moreno-Gonzalez, M.; Artuñedo, A.; Villagra, J.; Join, C.; Fliess, M. Speed-Adaptive Model-Free Path-Tracking Control for Autonomous Vehicles: Analysis and Design. *Vehicles* **2023**, *5*, 698–717. [CrossRef]
3. Lee, J.; Yim, S. Comparative Study of Path Tracking Controllers on Low Friction Roads for Autonomous Vehicles. *Machines* **2023**, *11*, 403. [CrossRef]
4. Lei, Z.; Ma, X.; Yuan, X.; He, C. Research on Automatic Driving Path Tracking Control of Open-Pit Mine Transportation Vehicles with Delay Compensation. *World Electr. Veh. J.* **2022**, *13*, 134. [CrossRef]
5. Thrun, S.; Montemerlo, M.; Dahlkamp, H.; Stavens, D.; Aron, A.; Diebel, J.; Fong, P.; Gale, J.; Halpenny, M.; Hoffmann, G.; et al. Stanley: The Robot That Won the DARPA Grand Challenge. In *The 2005 DARPA Grand Challenge*; Buehler, M., Iagnemma, K., Singh, S., Eds.; Springer: Berlin/Heidelberg, Germany, 2007; Volume 36, pp. 1–43. [CrossRef]
6. AbdElmoniem, A.; Osama, A.; Abdelaziz, M.; Maged, S.A. A Path-Tracking Algorithm Using Predictive Stanley Lateral Controller. *Int. J. Adv. Robot. Syst.* **2020**, *17*, 1–11. [CrossRef]
7. Liu, X.; Ou, J.; Yan, D.; Zhang, Y.; Deng, G. Path Tracking Control of Automated Vehicles Based on Adaptive MPC in Variable Scenarios. *IET Intell. Transp. Syst.* **2024**, *18*, 1031–1044. [CrossRef]
8. Cui, Q.; Ding, R.; Wei, C.; Zhou, B. Path-Tracking and Lateral Stabilisation for Autonomous Vehicles by Using the Steering Angle Envelope. *Veh. Syst. Dyn.* **2021**, *59*, 1672–1696. [CrossRef]
9. Sun, C.; Zhang, X.; Xi, L.; Tian, Y. Design of a Path-Tracking Steering Controller for Autonomous Vehicles. *Energies* **2018**, *11*, 1451. [CrossRef]
10. Rumetshofer, J.; Stolz, M.; Watzenig, D. A Generic Interface Enabling Combinations of State-of-the-Art Path Planning and Tracking Algorithms. *Electronics* **2021**, *10*, 788. [CrossRef]
11. Jung, H. Model-Based Hybrid Control of Pure Pursuit and Stanley Methods for Vehicle Path Tracking. *Sensors* **2025**, *25*, 6491. [CrossRef]
12. Hossain, T.; Habibullah, H.; Islam, R. Steering and Speed Control System Design for Autonomous Vehicles by Developing an Optimal Hybrid Controller to Track Reference Trajectory. *Machines* **2022**, *10*, 420. [CrossRef]
13. OpenStreetMap. Contributors OpenStreetMap. Available online: https://www.openstreetmap.org/ (accessed on 4 September 2026).
14. Savran, E.; Karpat, E.; Karpat, F. Fuel Cell Electric Vehicle Hydrogen Consumption and Battery Cycle Optimization Using Bald Eagle Search Algorithm. *Appl. Sci.* **2024**, *14*, 7744. [CrossRef]
15. Savran, E. Real-World Validated MVEM-Based Modeling and SoC-Dependent Driving Scenario Definition for a Parallel Hybrid Vehicle. *Proc. Inst. Mech. Eng. Part D J. Automob. Eng.* 2026, *in press* [CrossRef]
16. Cao, S.; Jin, Y.; Trautmann, T.; Liu, K. Design and Experiments of Autonomous Path Tracking Based on Dead Reckoning. *Appl. Sci.* **2023**, *13*, 317. [CrossRef]
17. Li, J.; Lou, J.; Li, Y.; Pan, S.; Xu, Y. Trajectory Tracking of Autonomous Vehicle Using Clothoid Curve. *Appl. Sci.* **2023**, *13*, 2733. [CrossRef]
18. Coulter, R.C. Technical Report CMU-RI-TR-92-01*Implementation of the Pure Pursuit Path Tracking Algorithm*; Technical Report CMU-RI-TR-92-01; Robotics Institute, Carnegie Mellon University: Pittsburgh, PA, USA, 1992.
19. Wang, L.; Chen, S.; Ren, H. An Accurate Trajectory Tracking Method for Low-Speed Unmanned Vehicles Based on Model Predictive Control. *Sci. Rep.* **2024**, *14*, 10739. [CrossRef]
20. Jeong, Y.; Yim, S. Model Predictive Control-Based Integrated Path Tracking and Velocity Control for Autonomous Vehicle with Four-Wheel Independent Steering and Driving. *Electronics* **2021**, *10*, 2812. [CrossRef]
21. Qiu, J.; Lin, D.; Tang, M.; Zhang, Q.; Song, H.; Zhao, Z. Trajectory Tracking of Unmanned Logistics Vehicle Based on Event-Triggered and Adaptive Optimization Parameters MPC. *Processes* **2024**, *12*, 1878. [CrossRef]
22. Wu, H.; Zhang, H.; Feng, Y. MPC-Based Obstacle Avoidance Path Tracking Control for Distributed Drive Electric Vehicles. *World Electr. Veh. J.* **2022**, *13*, 221. [CrossRef]

23. Yu, X.; Wang, H.; Teng, C.; Sun, X.; Chen, L.; Cai, Y. DGPR-MPC: Learning-Based Model Predictive Controller for Autonomous Vehicle Path Following. *IET Intell. Transp. Syst.* **2023**, *17*, 1992–2003. [CrossRef]
24. Yakub, F.; Abu, A.; Sarip, S.; Mori, Y. Study of Model Predictive Control for Path-Following Autonomous Ground Vehicle Control under Crosswind Effect. *J. Control Sci. Eng.* **2016**, *2016*, 6752671. [CrossRef]
25. Bautista-Camino, P.; Barranco-Gutiérrez, A.I.; Cervantes, I.; Rodríguez-Licea, M.; Prado-Olivarez, J.; Pérez-Pinal, F.J. Local Path Planning for Autonomous Vehicles Based on the Natural Behavior of the Biological Action-Perception Motion. *Energies* **2022**, *15*, 1769. [CrossRef]
26. Halaly, R.; Ezra Tsur, E. Autonomous Driving Controllers with Neuromorphic Spiking Neural Networks. *Front. Neurorobot.* **2023**, *17*, 4962. [CrossRef]
27. Hoffmann, G.M.; Tomlin, C.J.; Montemerlo, M.; Thrun, S. Autonomous Automobile Trajectory Tracking for Off-Road Driving: Controller Design, Experimental Validation and Racing. In *Proceedings of the American Control Conference*; IEEE: Piscataway, NJ, USA, 2007; pp. 2296–2301. [CrossRef]
28. Park, H.S.; Kim, M.S. Development of a Path Tracker Based on a 4WS Vehicle for Low-Speed Automated Driving Systems. *Appl. Sci.* **2025**, *15*, 3043. [CrossRef]

Disclaimer/Publisher's Note: The statements, opinions and data contained in all publications are solely those of the individual author(s) and contributor(s) and not of MDPI and/or the editor(s). MDPI and/or the editor(s) disclaim responsibility for any injury to people or property resulting from any ideas, methods, instructions or products referred to in the content.